INTERNATIONAL JOURNAL OF INTEGRATED ENGINEERING
ISSN: 2229-838X e-ISSN: 2600-7916

IJIE

Vol. 17 No. 2 (2025) 370-386
https://publisher.uthm.edu.my/ojs/index.php/ijie

Optimizing Solar Panel Cleaning with Kalman Filter-Enhanced Mobile Robotics

Hendi Purnata[1]*, Riyani Prima Dewi[1], Afrizal Abdi Musyafiq[1], Novita Asma Ilahi[1], Erna Alimudin[1], Saepul Rahmat[1]

[1] *Department Electro and Mechatronic Engineer,*
Cilacap State of Polytechnics, Jl. Dr. Soetomo No.1, Sidakaya Dua, Sidakaya,
Kec. Cilacap Sel., Kabupaten Cilacap, Jawa Tengah 53211, INDONESIA

*Corresponding Author: hendipurnata@pnc.ac.id
DOI: https://doi.org/10.30880/ijie.2025.17.02.030

Article Info

Received: 22 November 2024
Accepted: 18 July 2025
Available online: 8 August 2025

Keywords

Mobile robot, cleaning, panel surya, Kalman filter

Abstract

This study proposes the use of the Kalman filter method to accurately determine the position of the robot so that it can monitor the efficiency of the solar panels. This method is applied to the mobile solar panel cleaning robot, the Kalman filter is used to process data from the Inertial Measurement Unit (IMU) sensor on the robot specifically on the z-axis to accurately determine the position of the robot in the Cartesian coordinate system. The robot's performance tests show that the accuracy of the displacement measurement of the encoder corresponds to the pulse value. The test results showed that the use of the Kalman filter could significantly reduce the total error in the sensor data, namely when before using the Kalman filter, the total error from the reference axis gradient was 47.17 degrees, while by using the Kalman filter, the total error was 0.23 degrees, which means that the effectiveness of dust cleaning by the robot showed that the robot was able to reach the target coordinates with a high level of accuracy. Then, the mobile solar panel cleaning robot is taken simultaneously to monitor and maintain the efficiency of the solar panel in terms of dust and temperature drop. The efficiency of solar panels with a temperature drop of 5-6 degrees Celsius. The result of this study is a solar panel cleaning robot equipped with the Kalman filter algorithm to lower the temperature and clean dust. The total movement error of the robot was 0.73 for the X coordinates and 0.79 for the Y coordinates. The decrease in temperature had a positive effect on the increase in power by 2% from 85% to 87%. The results of this study show that the performance of the system is maintained in optimal conditions even though temperature fluctuations are successfully treated to increase the efficiency of the system, the temperature reduction according to the standard conditions (STC) is still not optimal, so further research and improvement is needed in the temperature reduction to achieve higher efficiency.

1. Introduction

In recent decades, there has been a clear growth in the use of solar energy, particularly in power generation through solar panels. Most countries in the world, both developed and developing. Where the growth of solar energy is achieved through the great expansion of solar panel installation, both on a small and large scale to serve

a large area and achieve sustainable development [1],[2],[3]. Solar panels are one of the new and renewable energy sources to generate electrical energy, which has many advantages, almost zero greenhouse emissions, flexible installation, ease and low maintenance costs and being environmentally friendly [4],[5],[6].

However, behind the excess, there are still problems that develop related to the efficient conversion of solar panels to electricity, some of which are the ambient temperature being too hot, cloudy, and dust accumulation which are considered the most important factors that have a negative effect on the performance of solar panels [7]. The temperature of a solar cell has a significant impact on the performance and efficiency of solar panels. When the temperature of the solar cell rises above the standard temperature of about 25 degrees Celsius, the efficiency of the solar panels tends to decrease. Previous research has shown that rising temperatures result in increased internal resistance and a decrease in the open voltage of the solar panel, which directly reduces the power that the panel can generate [8] Strategies to address the decrease in the efficiency of solar panels due to increased temperatures include the use of refrigerants or cooling systems to keep the temperature of the solar panel low during operation [9].

Previous research has also highlighted the importance of considering the temperature of solar cells in the development of mobile solar panel cleaning robots. Temperature management is a key factor in ensuring optimal performance of solar panels, especially when used in large solar power systems. Therefore, in addition to paying attention to factors such as dust accumulation and weather conditions, this study will also consider the influence of solar cell temperature in the process of cleaning solar panels using mobile robots [10].

Several studies have made cleaning robots such as in this research [11] in the cleaning process using mobile robots, which move remotely and automatically, so that in terms of cost it will be much cheaper, and in terms of work efficiency it is more efficient, because it does not require installation and disassembly of the static robot model (skeleton model), if the number of solar panels has a large capacity it will be cheaper and more efficient in its installation when in the plant. This research [12] in the cleaning process uses a mobile robot, which moves remotely and automatically, so that in terms of cost it will be much cheaper, and in terms of work efficiency it is more efficient, because it does not need to be installed and disassembled from the static robot model (Skeleton model), if the number of solar panels has a large capacity, it will be cheaper and more efficient in its installation when in the plant. Furthermore, this research [13] in the cleaning process uses mobile robots, which move remotely and automatically, so that in terms of cost it will be much cheaper, and in terms of work efficiency it is more efficient, because it does not require installation and disassembly and setting of the static robot model (frame model), if the number of solar panels has a large capacity, it will be cheaper and more efficient in its installation when in the plant.

From some studies it is suggested to use automatic control or use remote control, but in this control the most important problem is from the manufacture of complex mobile robots with the integration of several sensors, electronic and mechanical components. Several studies [14] are also to be able to overcome problems in mobile robots, namely in the study Making a locality of robots that are able to move based on coordinates using the odometric kinematic method produces an average error known when the robot moves is 0.399 cm, while the average error is actually 2.108 cm. In the study, [15] the problem faced was the estimation of the position of the robot when moving in a closed environment using sensor encoder and accelerometer by applying the Kalman filter. The Kalman filter is used to combine accelerometer and odometric sensor readings to estimate the robot's position and speed. The results showed an estimated position of the robot with an error of less than 0.2 meters, both for easy and difficult paths.

Research [16] on mobile robots deals with balance problems with fast, unstable, and nonlinear dynamics. The accelerometer sensor used is sensitive and noisy, and this problem is solved by applying a PID controller to control angle changes as well as a Kalman filter to reduce noise on the accelerometer sensor. The results showed that the Kalman filter successfully reduced the noise in the accelerometer sensor. The best parameters for the Kalman filter are R = 10 and Q = 0.01, while for PID controllers are Kp = 20, Ki = 1, and Kd = 20.

The research [17] addresses noise problems in the output of accelerometer and gyroscope sensors. The method used is the Kalman filter to reduce noise. The values of the Q and R parameters in the Kalman algorithm are varied to find the optimal value. The results showed that the Kalman filter successfully reduced the noise in the sensor, and the Q < R values provided the best results in reducing noise. The Kalman filter method has been used in previous studies, but it is used to filter the accelerometer data as in the study [14], [15], [16] .

However, most previous studies have utilized the Kalman filter only as an accelerator data filter or to stabilize the robot's movements. Not many have explicitly implemented the Kalman filter to improve the movement efficiency of solar panel cleaning robots based on position data in Cartesian coordinates while integrating them into the panel temperature monitoring system.

The main problems discussed in this study are the accumulation of dust on solar panels and temperature fluctuations that can affect the efficiency of solar sells. In this context, the aim of the research was to design the Kalman filter method to process data from IMU sensors on mobile solar panel cleaning robots. This method is expected to help mobile robots to move more efficiently over solar panels that have been defined in Cartesian coordinates. In addition, this study also aims to design a base station to monitor sensor data output, which is

Int. Journal of Integrated Engineering Vol. 17 No. 2 (2025) p. 370-386

expected to facilitate the process of analyzing and handling problems in mobile robots. Thus, the main objective of this study is to improve the cleaning efficiency of solar panels by overcoming the problem of dust accumulation and temperature fluctuations through the use of mobile robot technology and data processing using the Kalman filter method.

2. Methodology

This section will explain in detail the design and implementation of solar cell cleaning robots, including how the Kalman filter method is applied to the positioning of the robot to be used for solar panel cleaning. Before entering into the cleaning, the variable that affects the efficiency of the solar panel is the temperature as in the solar panel model below

2.1 Development of Solar Sell Cleaning Robot

In this sub-chapter, we will discuss the design, implementation, and effectiveness of the use of cleaning robots in maintaining the efficiency of solar panels. The main focus is on how cleaning robots can effectively remove dust as well as maintain optimal operating temperatures to maximize the performance and durability of solar panels.

For optimal efficiency and performance of solar panels, the design of the cleaning robot takes into account both technical and functional aspects. This robot is designed with technical capabilities as cleaning by sweeping dust and providing a flow that functions as a temperature lower.

2.1.1 Design

In this sub-chapter, the design of a cleaning robot is designed to solve the problem of dust and temperature on solar panels. The discussion will cover the main components of the robot, the cleaning mechanism, the cooling system, and the control technology used to ensure the robot can operate effectively.

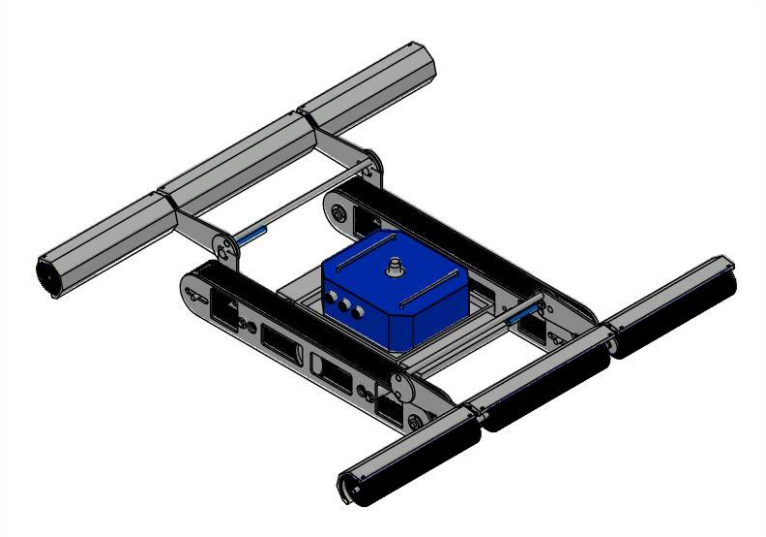

Fig. 1 *Robot design*

Figure 1. It is a robot design with several hardware installed into one part. The main part of this robot is using IMU sensors and the actuator uses a dc motor wrapped in a road wheel. The IMU sensor is useful for robot movement and robot movement with a road wheel that can move forward, backward and turn right and left. For temperature reduction by using a sprinkler.

2.1.2 Equipment Requirements

Based on the above design, various hardware supporting equipment is required to design and manufacture solar panel cleaning robots. The hardware can be seen from the following table:

Table 1 *Hardware requirements*

No	*Hardware*	Information
1.	Laptop/*PC*	To do programming, schematic creation and control of the robot through the base station.
2.	ESP 32	As the main controller, for robot logic and communication with base station.
3.	Raspberry Pico	Slave controller to read the sensor.
4.	Sensor rotary encoder	As input for the movement of the robot in the form of a measured distance of movement.
5.	Sensor IMU GY-87	As input for the movement of the robot in the form of the degree of direction facing the robot.
6.	Sprinkler	To spray water as a temperature dropper
7.	Motor DC	The main mover of the robot.
8.	Motor driver BTS 7960	Used to control DC motors.
9.	LCD I2C 16x2	Used to display the required information data.
10.	PCB	The main electrical place to be neater.
11.	Terminal block	To facilitate the distribution of power supply between components.
12.	Fuse	As a safety measure when there is an overcurrent, or a short circuit occurs.
13.	LiPo Battery	As the main source of robot power supply.

2.1.3 Robot Flow Diagram

Based on the design and supporting equipment required, the system can be implemented so that it can work according to its flow, as shown in the figure below.

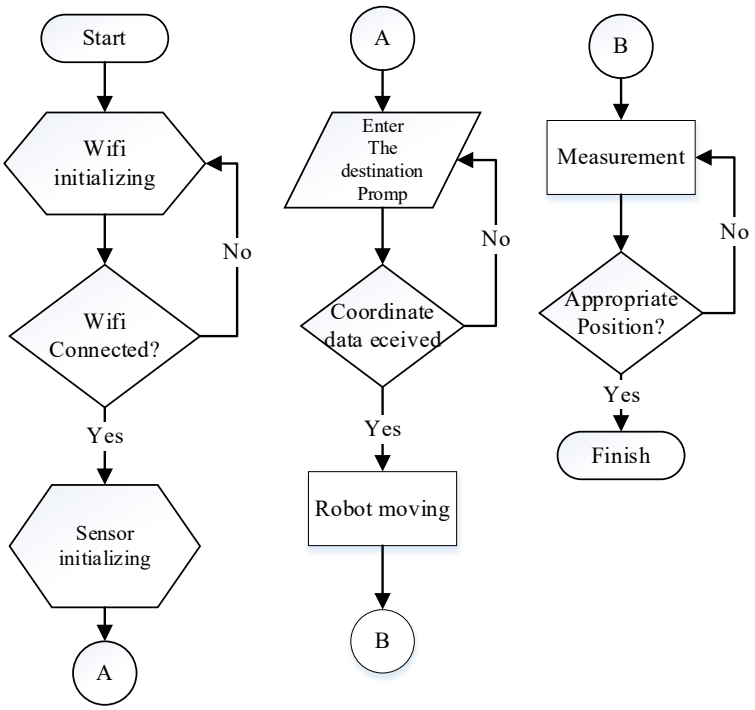

Fig. 2 *System flowchart*

Int. Journal of Integrated Engineering Vol. 17 No. 2 (2025) p. 370-386

In Figure 2, the flowchart describes the steps required to achieve the robot's goals. First, when the robot is first turned on, it will initialize the Wi-Fi connection. Once connected, the robot will initialize the sensor and wait for the target command data entered by the user. After receiving the command data, the robot will move towards the target until it reaches the goal. Measurements are taken to verify the position of the robot. If the position matches the destination setpoint, the steps are complete. However, if it does not match, the system will return to the measurement position and re-evaluate. This flowchart helps visualize the process of achieving the robot's target setpoint at Global Coordinates.
After understanding the flowchart, the next step is to implement it in the control system according to the control system diagram block shown in the following image.

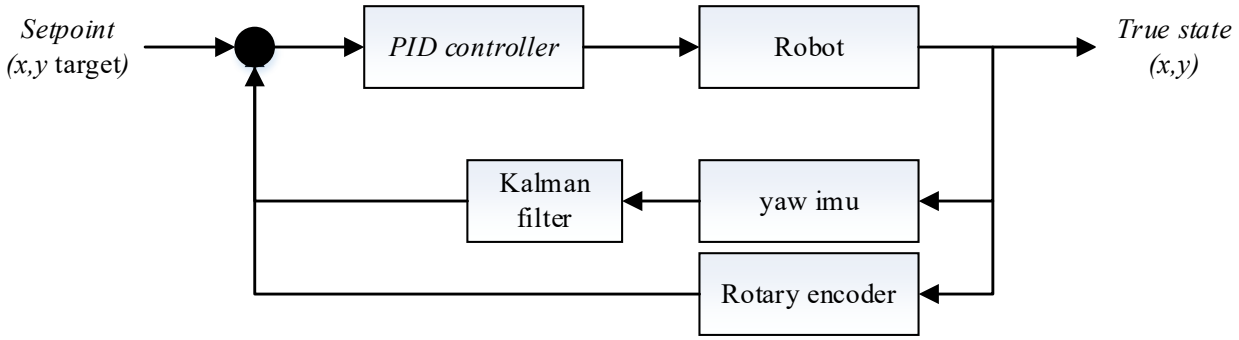

Fig. 3 *Controller block diagram*

Figure 3 is a block diagram that illustrates the system starting by setting a goal setpoint. The setpoint is then processed by the PID controller as the initial input to drive the actuator in the form of a DC motor. The robot then moves according to the set setpoint. The sensor readings are used as the robot's position feedback. The data from the sensor is processed using the Kalman filter algorithm so that the received data can accurately match field conditions.

After understanding the drawings, devices used, and block diagrams, we will next discuss the overall wiring diagram, which includes the power circuit, sensors, and actuators. In the series Figure 5, the entire series is described in a robot system with three omnidirectional wheels. The combination of the motor circuit and the sensor circuit has an important role in controlling movement and maintaining the performance of the robot. The motor circuit, which consists of a BTS7960 motor driver and a DC motor, is responsible for driving the robot.

Meanwhile, the sensor circuit starts from a 12V power source and goes through a voltage conversion using a stepdown component to 5V. The sensor array serves to provide the right voltage to components such as connected sensors and microcontrollers. With the combination of these two circuits, the system is able to control the speed, direction of rotation, and maneuvering of the robot. In addition, the system also allows data capture and interaction with the surrounding environment through sensors.

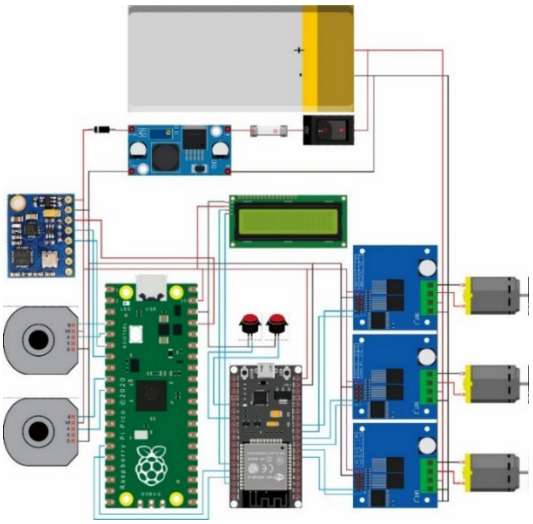

Fig. 4 *Network as a whole*

Once properly installed, to make sure the robot is up to its purpose, focus on designing the Kalman filter. The Kalman filter formula needs to be adjusted to fit the purpose of this final project. The Kalman filter formula here is used to process data from the GY-87 IMU sensor to obtain z-axis data. This data will be a reference in determining the direction facing the robot when navigating in a predetermined arena. Here is the modified Kalman filter formula:

Predictions:

$$\hat{x}_k^- = \hat{x}_{k-1} + dt * newRate \quad (1)$$

$$P_k^- = A * P_{k-1} * A' + Q\_gyro * dt \quad (2)$$

Correction:

$$S = P_k^- + R\_angle \quad (3)$$

$$K_k = P_k^- / S \quad (4)$$

$$\hat{x}_k = \hat{x}_k^- + K_k * (newAngle - \hat{x}_k^-) \quad (5)$$

$$P_k = (1 - K_k) * P_k^- \quad (6)$$

where:

- $\hat{x}_k^-$ = Estimation of the state variable in the Kth iteration after the prediction stage.
- $\hat{x}_{k-1}$ = Estimation of the state variable in the previous iteration (before the prediction stage).
- dt = the time difference between the current iteration and the previous iteration.
- $newRate$ = the actual angular acceleration measured from the gyro sensor.
- P_k^- = covariance matrix at the k iteration after the prediction stage.
- A = a transition matrix that defines how a state variable evolves in a single iteration.
- P_{k-1} = covariance matrix in previous iterations (before the prediction stage).
- A' = transpose of the transition matrix, but the transition matrix is ignored because the prediction is based on the actual rate of change obtained from the gyro sensor.$AnewRate$
- Q_gyro = covariance representing uncertainty in gyro changes.
- S = total uncertainty that includes the uncertainty of the prediction stage plus the uncertainty of the measurement data $(P_k^-)(R\_angle)$.
- K_k = Kalman Gain on the kth iteration after the correction stage.
- $newAngle$ = the actual angle measured from the sensor (measurement data).
- $\hat{x}_k$ = Estimated state variables in the k iteration after the correction stage.
- P_k = covariance matrix in the k iteration after the correction stage.
- P_k^- = covariance matrix at the k iteration after the prediction stage.

Int. Journal of Integrated Engineering Vol. 17 No. 2 (2025) p. 370-386

Then in its application in the program code, the flow of the program can be seen in the flowchart below.

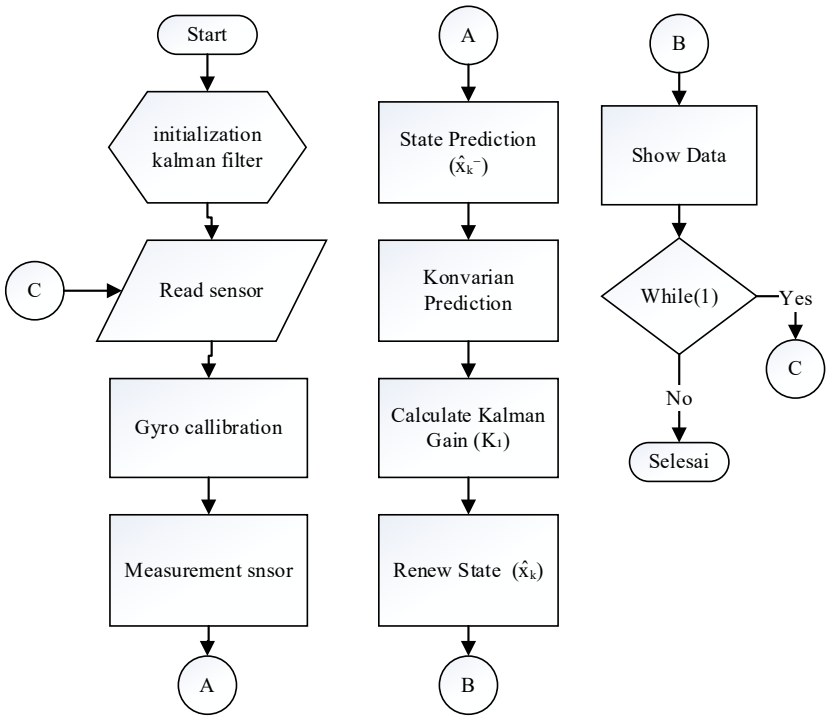

Fig. 5 *Flowchart program Kalman filter*

Figure 5 is a *Flowchart* of the Kalman filter program code where the process begins with the initialization of the Kalman filter and the calibration of the gyro on the GY-87 IMU sensor to remove the offset. Next, the gyro data is read from the sensor and the gyro speed is calculated. Then, the algorithm performs state predictions and covariance matrix predictions based on previously calculated gyro data. From these predictions, Kalman Gain is also calculated to combine prediction data and actual data.$(gyro\_z)$ $(\hat{x}_k^-)(P_k^-)$ (K_1)

After that, the algorithm updates the state and the covariance matrix based on the gyro's actual data. Valid gyro data will trigger an update, while invalid gyro data will cause a backflow to the gyro data reading from the sensor. After the update is complete, the estimated gyro data and yaw angle are displayed as $(\hat{x}_k)(P_k)Output$ of the algorithm.

The final stage of this research is the implementation of a remote control, where a base station is created as a Human-Machine Interface (HMI) that will control the solar panel cleaning robot from a computer or other device.

Base station Robots are used to communicate with robots, such as monitoring robot movements, and giving commands to robots. This base station is built with the Qt framework and the python programming language, the choice of using Pyqt5 due to its ease of use, and the complete features in the python programming language itself. The display on the base station can be seen in Figure 6.

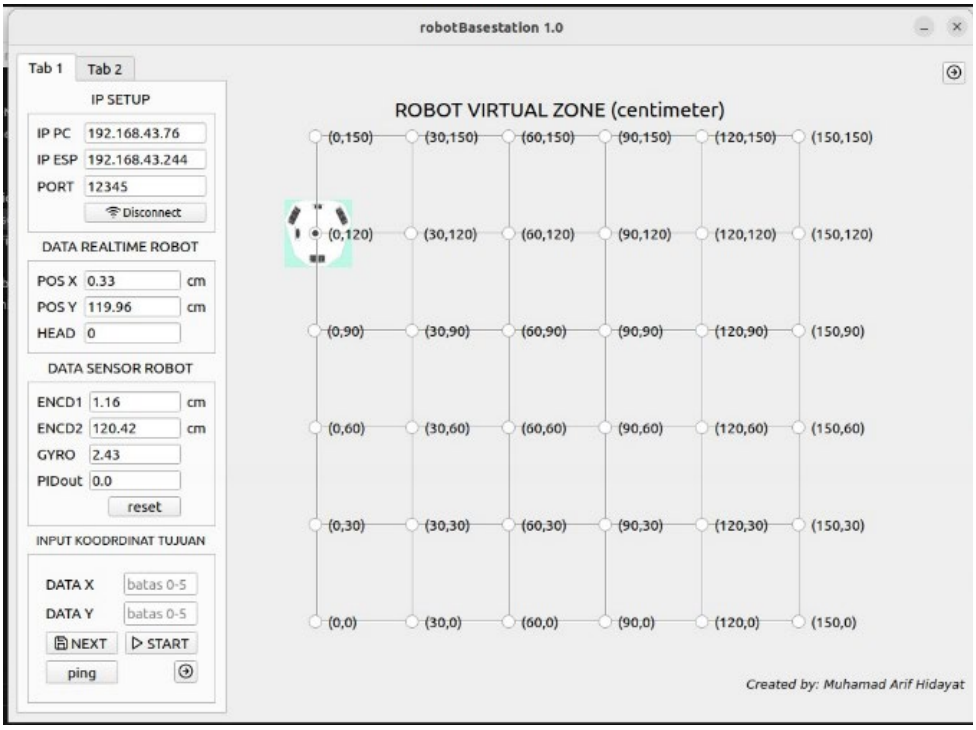

Fig. 6 *Base station robot*

In the base station, there are several features such as changing IP addresses, Wi-Fi address changes, monitoring robot sensor data, real-time monitoring of robot position data, and sending commands where the robot will run. Thus, the methodological stages described above will be the basis for conducting tests and analyses which will be described in the results and discussion section.

2.2 Solar Panels

Solar sales are the main key to the change from heat energy to electrical energy. In some cases, semiconductors are used as solar cell materials. Energy conversion consists of the absorption of photon energy that results in electron-hole pairs in semiconductors and carrier separation. PN Junction is used for load separator. The Solar sell model that will be used as in this sub-chapter.

2.2.1 Model Solar Sell

The solar sell model used is to use a single diode with a structure consisting of current and diodes arranged in parallel and also include the effect of resistance connected in series.

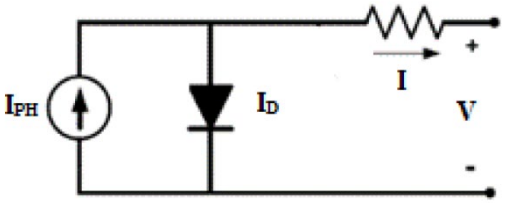

Fig. 7 *Diagram series on photovoltaic cells*

The mathematical model of photovoltaic cells varies with short circuit current and open circuit voltage obtained from the datasheet. Increased accuracy can be generated from temperature models and reliance on semiconductor band gap energy. Using the model in general by applying Kirchhoff's law to the common nodes of the current source, diode and resistance series (), the current of the solar panel, I, can be derived by:$(I_{sc})(V_{oc})RS$

$$I = I_{PH} - I_D \tag{7}$$

Int. Journal of Integrated Engineering Vol. 17 No. 2 (2025) p. 370-386

$$I = I_{PH} - I_D\left(\exp\left[\frac{V + R_S I}{U_T}\right] - 1\right) \quad (8)$$

Where:
I : Solar module output current (A),
V : Solar module output voltage (V),
I_{PH} : Photo-current of the panel surya module (A),
I_S : Diode reverse saturation current (μA),
R_S : Series resistance associated with the cell (mΩ),
U_T : Thermal voltage [UT = nKB T/q],
n : Diode ideality factor, its value ranges between 1 and 2,
q : Electron charge [q = 1.602 × 10−19 C],
K_B : Boltzman's constant [= 1.38 × 10−23 J/K],
T : Temperature (K).

Photocurrent depends on the temperature on:

$$I_{PH} = I_{PH0}\left(1 + K_0(T - T_0)\right) \quad (9)$$

$$I_{PH0} = \left(\frac{I_{sc0}}{G_0}\right)G \quad (10)$$

$$K_0 = \left(\left(I_{sc,T_1} - I_{sc,0}\right) - (T_1 - T_0)\right) \quad (11)$$

Where:

- G : = Irradiance level (), W/m^2
- G_0 = Irradiance level pada Standard Test Conditions (STC) Dimana spectrum rata-rata pada AM 1.5 is used, the irradiance G0 is normalized to 1 sun = 1000 W/m^2, and the cell temperature T0 is equal to 25°C.
- I_{sc} = Short-circuit current of the module,
- $I_{sc,0}$ = Short-circuit current of the module at .T_0

Temperature depends on the saturation which is calculated according to the following equation:

$$I_s = I_{s,0}\left(\frac{T}{T_0}\right)^{3/n} \exp\left(-\left[\left(\frac{qE_g}{nK_B}\right)\left[\left(\frac{1}{T}\right) - \left(\frac{1}{T_0}\right)\right]\right]\right) \quad (11)$$

$$I_s, 0 = \frac{I_{sc,0}}{\left[\exp\left(\frac{V_{oc,0}}{U_{T0}}\right) - 1\right]} \quad (12)$$

$$E_G(T) = E_{g0} - \left[\frac{\alpha T^2}{(T + \beta)}\right] \quad (13)$$

Where:

- $I_{S,0}$: = Diode reverse saturation current at STC,
- $V_{oc,0}$ = Open-circuit voltage of the module at T0,
- E_g = Band-Gap energy of the semiconductor used in the cell sesuai dengan material konstanta.α dan β

The energy of the Band Gap of semiconductors decreases with increasing temperature, and its temperature dependence is well modeled. The most influential parameters of this model are voltage, irradiation and temperature. The parameters used in this study are:

Table 2 *Model solar sell*

Name	Technical Specifications
Model	ST200W-32-M
Cell Type	Polycrystalline silicon
Maximum Power $[P_{max}](W)$	200
Voltage at Maximum Power $[V_m](V)$	18.24
Current at Maximum power $[I_m](A)$	10.96
Short-circuit current $[I_{sc}](A)$	11.62
Open-circuit voltage $[V_{oc}](V)$	21.8
Net Weight (KGS)	21
Size	1290*760*30MM

2.2.2 Solar Sell Efficiency

Solar sell is generated from the power of sunlight which can be said to be on sneeze energy. However, the output of solar panels is limited. To know the calculation of panel efficiency which means greater effective for the project. Solar sell efficiency where the power from the plant is compared to the total power input specifically, namely the amount of sunlight that increases on the panels. The efficiency of solar panels is calculated from watts per unit of panel power. The efficiency of solar panels is as in the following equation:

$$Efficiency\ (\%) = \frac{Pmax}{(Area\ \times 1000\ W/m^2)} \times 100 \tag{14}$$

Where

- STC = irradiance $1000w/m^2$
- $Pmax$ = Max Panel power (w)
- $Area$ = Panel Area $()m^2$

To maximize the energy conversion efficiency of solar panels, it is important to understand the various variables that affect them. The efficiency of solar panels is affected by the area of the panel, Standard Test Conditions (STC) conditions, temperature, and dust. The area of the solar panel determines how much sunlight can be captured and converted into electrical energy. The STC conditions, which include a temperature of 25°C, radiation of 1000 W/m^2, and an air mass of 1.5, are used as a reference to measure the performance of solar panels under optimal conditions. The two main variables that have a significant impact on the efficiency of solar panels are temperature and dust. The temperature of the solar cell has a direct effect on the performance of the solar panel, where the increase in temperature above the optimal operating temperature can reduce the efficiency of the panel. This is due to changes in the electrical characteristics of solar cells at high temperatures, resulting in a decrease in voltage and overall efficiency. Dust that accumulates on the surface of solar panels is also an important factor that reduces efficiency, as it blocks sunlight from reaching the solar cells, thereby reducing the amount of energy that can be converted into electricity.

2.2.3 Temperature

When the temperature of the solar cell increases, the efficiency of the solar cell generally decreases. This is due to an increase in the concentration of intrinsic carriers, which affects the open circuit voltage (Voc) and overall power output. Efficiency can be estimated by:

$$\eta = \eta_{STC} \times \left(1 - \beta \times (T - T_{STC})\right) \tag{15}$$

Where η_{STC} is the efficiency at the standard test conditions, β is the temperature coefficient, T is the temperature of the solar cell and T_{STC} the temperature at the STC

2.2.4 Dust

Dust reduces the amount of sunlight that reaches the cell, thereby reducing the power output. The impact of dust varies with the type of dust and the duration of exposure. The reduction in efficiency due to dust can be modeled by:

$$\eta = \eta_{clean} \times (1 - k \times D) \tag{16}$$

Where η_{clean} is the efficiency of a clean panel, is the constant representing the impact of dust, and D is the density of dust. The combined effect of temperature and dust on the efficiency of solar panels can be expressed as a multiplication function of the two factors. Assuming these effects are independent, the overall efficiency of the$k$

$$\eta_{overall} = \eta_{STC} \times \big(1 - \beta \times (T - T_{STC})\big)(1 - k \times D) \quad (17)$$

To overcome the problem of temperature and dust on solar panels, the use of cleaning robots is an innovative and efficient solution. The robot is not only tasked with cleaning the dust that accumulates on the surface of the panels, but is also equipped with a system that can maintain an optimal operating temperature of 25 degrees Celsius. With the right technology, the cleaning robot is able to carry out cleaning automatically and keep the temperature of the panel stable, thus ensuring that the solar panels operate at their best conditions and produce maximum energy.

3. Results and Discussion

For testing, some aspects that will be tested include the overall performance of the robot, the ability of sensors and actuators to move the robot, the Kalman filter, and the connection between the base station and the robot in the process of cleaning solar panels. In addition, the cleaning results will also be observed to assess the efficiency of the solar panels after the cleaning process is carried out.

3.1 Performa Robot

3.1.1 Sensor and Actuator Capabilities

In this test, the data taken from the rotary encoder sensor in the form of pulses (pulses) is converted into units of length (cm). The test was carried out by manually moving the robot forward, backward, right, and left. There are two rotary encoders installed: rotary encoder 1 is used to measure the displacement of the X Coordinates, and rotary encoder 2 is installed to measure the displacement of the Y Coordinates.

Table 3 *Comparison of robot distances*

No	Distance	Axis X (Pulse Encoder 1)	Axis Y (Pulse Encoder 2)
		Forward	
1	30	0.1	30.22
2	60	0.12	60.07
3	90	1.02	90.37
4	120	0.13	120.64
5	150	1.05	150.67
		Backward	
1	-30	-0.08	-30.13
2	-60	-1.04	-60.66
3	-90	-0.03	-90.21
4	-120	-0.12	-120.54
5	-150	-0.01	-150.05
		Turn Right	
1	30	30.54	0.53
2	60	61.51	0.22
3	90	90.2	1.07
4	120	120.07	0.12
5	150	150.92	0.46
		Turn Left	
1	-30	-30.23	-0.21
2	-60	-59.96	-0.43
3	-90	-90.21	-0.98
4	-120	-119.89	0.07
5	-150	-150.07	0.02

From the test data, when the robot moves forward with distances of 30 cm, 60 cm, 90 cm, 120 cm, and 150 cm, the pulse value on the X axis is relatively small compared to the pulse value on the Y axis.

The pulse value on the Y axis shows a consistent increase with the distance traveled, indicating that encoder 2 (Y axis) works well in measuring forward displacement. When the robot moves backwards at the same distance (-30 cm, -60 cm, -90 cm, -120 cm, and -150 cm), a similar pattern is observed on the Y-axis, with a negative pulse value consistent with the direction of backward movement.

As in forward motion, the pulse value on the X axis remains small, indicating that the main motion remains on the Y axis. When the robot moves to the right at distances of 30 cm, 60 cm, 90 cm, 120 cm, and 150 cm, the pulse value on the X axis shows an increase consistent with the distance traveled, while the pulse value on the Y axis remains small. This corresponds to the expectation that the main displacement occurs on the X axis.

The data shows that encoder 1 (X-axis) is effective in measuring displacement to the right. When the robot moves to the left at the same distance (-30 cm, -60 cm, -90 cm, -120 cm, and -150 cm), the pulse value on the X-axis shows a negative value consistent with the direction of movement to the left.

As in the right movement, the pulse value on the Y axis remains small, indicating that the main displacement remains on the X axis. The pulse value generated by the encoder is closely related to the distance traveled by the robot on the appropriate axis.

The small pulse value on the axis that is not the main direction of movement indicates a slight deviation or error that may be caused by mechanical imperfections or settings in the encoder, but this deviation is relatively small and insignificant. Rotary encoder 1 is effective in measuring displacement on the X axis, while rotary encoder 2 is effective in measuring displacement on the Y axis.

The pulse value generated by the encoder is directly proportional to the distance traveled, indicating good accuracy in displacement measurements. Small deviations on the axis that are not the main direction of movement can be negligible in this context but can be an area for further improvement in calibration and mechanical settings.

3.1.2 Kalman Filter

The test results at this stage were obtained by comparing the output data from the GY-87 IMU sensor with the data from the compass. The test is carried out in two stages: first, testing the sensor data before using the Kalman filter method, and second, testing the sensor data after using the Kalman filter method where the total error using the Kalman filter is greatly reduced, which means that this method is very effective. The test data can be seen in Table 4.

Table 4 *Comparison of robot distances*

No.	Reference (degree)	Before KF (degree)	After KF (degree)	*Error* before KF	*Error* after KF
1	0	0.01	0.01	0.01	0.01
2	30	40.37	29.68	10.37	-0.32
3	60	40.23	60.33	-19.77	0.33
4	90	36.88	90.07	-53.12	0.07
5	120	58.65	120.32	-61.35	0.32
6	150	75.52	149.87	-74.48	-0.13
7	180	125.76	179.89	-54.24	-0.11
Total *error*				47.17	0.23

Int. Journal of Integrated Engineering Vol. 17 No. 2 (2025) p. 370-386

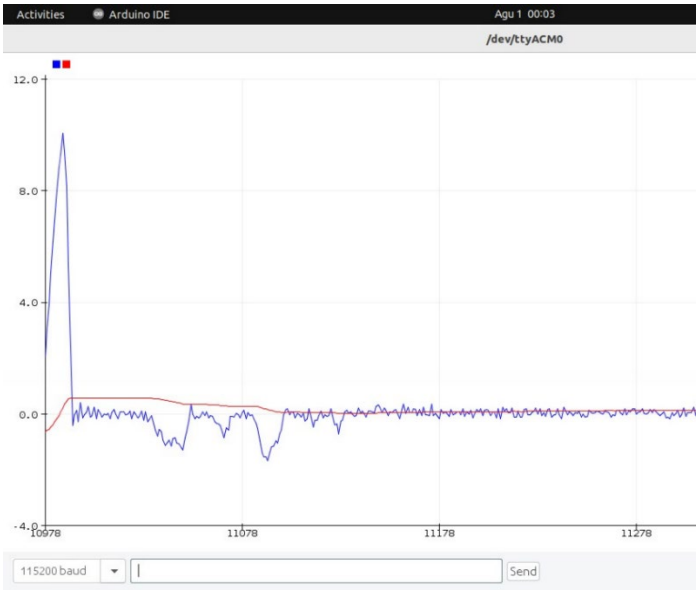

Fig. 8 *IMU data comparison of the cleaning robot*

Connection testing begins by entering the laptop's IP address and the ESP32 IP address, as well as the ports used. Then, the "connect" button on the base station interface is pressed. If the connection is successful, the "connect" button will change to "disconnect". The experiment was carried out 10 times with a variation of the distance between the base station and the Wi-Fi hotspot.

Connection tests showed that the system was able to maintain consistent and fast connectivity between the base station and the robot at various Wi-Fi distances, ranging from 2 meters to 12 meters. Each time the distance was tested, the connection was successfully established in less than a second, showing that the system can be relied upon to efficiently connect devices even over longer distances. These results indicate the system's ability to respond quickly and maintain connection stability, which is important for robot operations in scenarios that require remote control.

After the distance and also the test of the coordinate data, this test is carried out to find out whether the data is sent correctly from the base station to the robot. The test was carried out 10 times by sending the command data of the target Coordinate X and the target Coordinate Y. The command was carried out using several tools available on the base station that had been created.

3.1.3 Effectiveness in Dust and Temperature Cleaning

Dust and temperature cleaning is carried out on solar panels with a size of 120 x 53 x 3.5 cm which is base station according to the size to clean the dust. This test is carried out by determining the coordinate points so that they can be cleaned thoroughly. The image of the base station is shown in the image below 9 where to move the robot you can enter the Coordinate value in the "DESTINATION COORDINATE INPUT" section on the menu at the base station marked with a yellow box with input values between 0 - 120 and you can also directly press the Coordinates in the "ROBOT VIRTUAL ZONE" menu. The test results were obtained by running the robot in the test arena, by entering the coordinates of the robot's purpose to clean the dust on the solar panel and provide a treatment with water to reduce the temperature of the solar panel through the base station.

Table 5 *Cleaning destination coordinates*

No.	Destination coordinates					
	Reference		Result		*Error*	
	X	And	X	And	X	And
1	0	120	0.7	120.11	-0.7	-0.11
2	120	120	121.2	119.57	-1.2	0.43
3	120	0	120.4	-0.89	-0.4	0.89
4	0	0	-0.24	1.23	0.24	-1.23
			Total *error*		0.73	0.79

This test aims to measure the accuracy of the robot in achieving the set goal coordinates. The robot is run in the test arena by entering the destination coordinates, then the position achieved by the robot is compared to the reference coordinates. Error is calculated as the difference between the destination coordinates and the position result achieved by the robot. The total error in this test was 0.73 for the X coordinates and 0.79 for the Y coordinates. A small error in the position results indicates the effectiveness of the robotic navigation system in reaching the set coordinates.

3.2 Solar Panel Efficiency

This test aims to see how efficient the solar panels are after dust cleaning and temperature cooling by robots. Efficiency is measured before and after cleaning to determine the improvement in the performance of the solar panel. The test was carried out on Thursday, May 2, 2024 at the Cilacap State Polytechnic at 12.20-14.20 or 2 hours apart with a span of 20 minutes 1 time in order to clean and maintain the temperature. The data in this study can be seen in the graph below.

Table 6 *Cleaning destination coordinates*

Time	Before Treatment(^{0}C)	Temperature(^{0}C)
12.20	41,35	32,19
12.40	42	30,9
13.20	40,06	30,75
13.40	40,5	30,75
14.00	39	31,25
14.04	39,12	31,28
14.08	37,88	31,12
14.12	38,44	31,06
14.20	39,41	31

Data analysis showed that the temperature before treatment was in the range of 37.88°C to 42°C, while the temperature after treatment dropped significantly to 30.75°C to 32.19°C. This temperature drop pattern was consistent during the test period from 12:20 to 14:20 with a time interval of 20 minutes. This shows that the treatment is effective in lowering the temperature and keeping it at a lower and more stable level. The treatment applied, i.e. cleaning the dust and flushing the water, succeeded in lowering the initial high temperature to a lower and stable level within the specified time interval. This test proved that a time span of 20 minutes was effective enough to reach and maintain the desired temperature, demonstrating the success of the method used in the testing at the Cilacap State Polytechnic.

The data above shows that it can decrease but has not been pointed to be able to maintain a temperature of 25 degrees Celsius. It compares the power obtained before and after using the dust cleaning treatment and providing water to lower the temperature.

Power data before and after dust cleansing. The temperature testing process which was carried out on Thursday, May 2, 2024 at the Cilacap State Polytechnic aimed to evaluate the effectiveness of dust cleaning and watering methods in lowering temperatures. Temperature data before and after treatment was collected at specific time intervals to observe the changes that occurred. Here is a breakdown of the temperature data measured before and after treatment, showing how dust cleaning and watering affect the temperature significantly. The results of this measurement provide a clear picture of the effectiveness of the method used in maintaining temperature stability.

Int. Journal of Integrated Engineering Vol. 17 No. 2 (2025) p. 370-386

Table 7 *Power comparison*

Time	Before cleaning			After cleaning		
	Voltage (V)	Current (A)	Power (P)	Voltage (V)	Current (A)	Power (P)
12.20	17,42	9,22	160,6124	17,75	9,34	165,785
12.40	17,02	8,43	143,4786	17,21	9,16	157,6436
13.20	17,4	8,67	150,858	17,61	9,35	164,6535
13.40	17,28	8,01	138,4128	17,96	9,21	165,4116
14.00	17,58	7,7	135,366	18,07	8,7	157,209
14.04	17,86	7,12	127,1632	17,95	9,63	172,8585
14.08	17,53	8,12	142,3436	18,01	9,04	162,8104
14.12	17,52	7,74	135,6048	17,99	8,99	161,7301
14.20	17,14	7,43	127,3502	17,95	9,07	162,8065

The analysis of the data provided regarding voltage, current, and power before and after cleaning showed a significant increase after the cleaning process was carried out. Before cleaning, the average voltage recorded was about 17.35 V, the current was about 7.88 A, and the power was about 136.63 W. After cleaning, there was a noticeable increase, with the average voltage rising to about 17.98 V, the current rising to about 9.14 A, and the power rising to about 162.39 W. This indicates that the cleaning successfully improved the performance of the device, which is reflected in the increase in voltage, current, and power. However, to understand more deeply the impact of cleaning, it is necessary to pay attention to the temperature effect (STC) mentioned as 25 degrees Celsius. Information about the temperature before and after cleaning can help clarify the extent to which temperature affects the observed differences.

So the efficiency of the solar panel as in equation (12) and for the power efficiency as in equation (9) With is 89% and 0.3% per degree Celsius while we take the temperature here from the temperature before and after, is a constant that represents the dust impact of 2%, and D is the dust density of 3%, then the result can be seen in the following table.

Table 8 *Power comparison*

Time	Before at Treatment			After Treatment		
	Temperature ()℃	Daya (%)	Overall (%)	Temperature ()℃	Daya (%)	Overall (%)
12.20	41,35	80	85	32,19	83	87
12.40	42	72	84	30,9	79	87
13.20	40,06	75	85	30,75	82	87
13.40	40,5	69	85	30,75	83	87
14.00	39	68	85	31,25	79	87
14.04	39,12	64	85	31,28	86	87
14.08	37,88	71	86	31,12	81	87
14.12	38,44	68	85	31,06	81	87
14.20	39,41	64	85	31	81	87
		70	85		82	87

Comparison between the temperature before and after the treatment showed significant changes. The temperature before treatment ranges from 37.88°C to 42°C, while after treatment, the temperature decreases to 30.75°C to 32.19°C. With a drop of 5-6 degrees Celsius, the treatment successfully lowers the temperature effectively. In addition, it can be seen that the power before treatment ranges from 64% to 80%, but after treatment, the power remains stable at 87%. This shows that the decrease in temperature has a great effect on the increase in power. The overall efficiency also remained stable at an average of 87% after treatment. From this data, it can be seen that focusing on temperature drops is the key to increasing maximum power and efficiency. However, to achieve higher efficiency and get closer to standard conditions (STC), it is necessary to focus on lowering the temperature by up to 25 degrees Celsius. Although the treatment has succeeded in improving

efficiency, the temperature reduction according to the STC is still not optimal, so further improvements in temperature reduction in solar panels can be the focus of further research to achieve higher efficiency.

4. Conclusion

The result of this study is a solar panel cleaning robot equipped with the Kalman filter algorithm to lower the temperature and clean dust. The total movement error of the robot was 0.73 for the X coordinates and 0.79 for the Y coordinates. The decrease in temperature had a positive effect on the increase in power by 2% from 85% to 87%. The results of this study show that the system performance is maintained in optimal conditions even though temperature fluctuations are successfully treated to increase system efficiency, temperature reduction according to standard conditions (STC) is still not optimal, so further research and improvement are needed on temperature reduction to achieve higher efficiency.

Acknowledgement

We would like to express our deepest gratitude to Cilacap State Polytechnic for its generous financial support and invaluable resources, which are very important for the success of our research. We would like to express our special gratitude to the lecturers and students for the achievement of this paper. This research would not have been possible without the joint efforts and encouragement of all colleagues and big names of the Cilacap State Polytechnic.

Conflict of Interest

We declare that in the research and preparation of this paper there is no conflict of interest from one or more parties involved.

Author Contribution

Problems and design: *Hendi Purnata, Afrizal Abdi Musyafiq;* ***Data input and processing****: Riyani Prima Dewi, Novita Asma Ilahi;* ***draft manuscript preparation:*** *Erna Alimudin, Saepul Rahmat. All authors reviewed and wrote the results for this study.*

References

[1] T. Salamah *et al.*, "Effect of dust and methods of cleaning on the performance of solar PV module for different climate regions: Comprehensive review," *Science of The Total Environment*, vol. 827, p. 154050, 2022, doi: https://doi.org/10.1016/j.scitotenv.2022.154050.

[2] S. Fan, W. Liang, G. Wang, Y. Zhang, and S. Cao, "A novel water-free cleaning robot for dust removal from distributed photovoltaic (PV) in water-scarce areas," *Solar Energy*, vol. 241, pp. 553–563, 2022, doi: https://doi.org/10.1016/j.solener.2022.06.024.

[3] S. M. Shalaby *et al.*, "Reverse osmosis desalination systems powered by solar energy: Preheating techniques and brine disposal challenges – A detailed review," *Energy Convers Manag*, vol. 251, p. 114971, 2022, doi: https://doi.org/10.1016/j.enconman.2021.114971.

[4] A. H. Natural *et al.*, "Management of potential challenges of PV technology proliferation," *Sustainable Energy Technologies and Assessments*, vol. 51, p. 101942, 2022, doi: https://doi.org/10.1016/j.seta.2021.101942.

[5] D. Adak, R. Bhattacharyya, and H. C. Barshilia, "A state-of-the-art review on the multifunctional self-cleaning nanostructured coatings for PV panels, CSP mirrors and related solar devices," *Renewable and Sustainable Energy Reviews*, vol. 159, p. 112145, 2022, doi: https://doi.org/10.1016/j.rser.2022.112145.

[6] A. El Hammoumi, S. Chtita, S. Motahhir, and A. El Ghzizal, "Solar PV energy: From material to use, and the most commonly used techniques to maximize the power output of PV systems: A focus on solar trackers and floating solar panels," *Energy Reports*, vol. 8, pp. 11992–12010, 2022, doi: https://doi.org/10.1016/j.egyr.2022.09.054.

[7] B. Zou, J. Peng, S. Li, Y. Li, J. Yan, and H. Yang, "Comparative study of the dynamic programming-based and rule-based operation strategies for grid-connected PV-battery systems of office buildings," *Appl Energy*, vol. 305, p. 117875, 2022, doi: https://doi.org/10.1016/j.apenergy.2021.117875.

[8] Q. Gu, S. Li, W. Gong, B. Ning, C. Hu, and Z. Liao, "L-SHADE with parameter decomposition for photovoltaic modules parameter identification under different temperature and irradiance," *Appl Soft Comput*, vol. 143, p. 110386, 2023, doi: https://doi.org/10.1016/j.asoc.2023.110386.

[9] D. Wang *et al.*, "A study on frost and high-temperature resistance performance of supercooled phase change material-based flat panel solar collector," *Solar Energy Materials and Solar Cells*, vol. 239, p. 111665, 2022, doi: https://doi.org/10.1016/j.solmat.2022.111665.

[10] R. K. Rajamony *et al.*, "Progress in research and technological developments of phase change materials integrated photovoltaic thermal systems: The allied problems and their mitigation strategies," *Sustainable Materials and Technologies*, vol. 40, p. E00921, 2024, doi: https://doi.org/10.1016/j.susmat.2024.e00921.

[11] S. Mousavi and G. Farahani, "Introducing a new method of automatic cleaning of the PV array surface using a suction robot," *Mechatronics*, vol. 85, p. 102845, 2022, doi: https://doi.org/10.1016/j.mechatronics.2022.102845.

[12] X. Li and X. Li, "Development of following robot for supplying power to solar panel cleaning robot," *Industrial Robot: the international journal of robotics research and application*, vol. 49, no. 1, pp. 88–95, Jan. 2022, doi: 10.1108/IR-03-2021-0055.

[13] T. Li *et al.*, "A Mobile Robot Design for Efficient and Large-Scale Solar Panel Cleaning," in *2022 IEEE International Conference on Robotics and Biomimetics (ROBIO)*, 2022, pp. 70–75. doi: 10.1109/ROBIO55434.2022.10011850.

[14] P. K. Panigrahi and S. K. Bisoy, "Localization strategies for autonomous mobile robots: A review," *Journal of King Saud University - Computer and Information Sciences*, vol. 34, no. 8, Part B, pp. 6019–6039, 2022, doi: https://doi.org/10.1016/j.jksuci.2021.02.015.

[15] X. Xu, Y. Sun, X. Tian, L. Zhou, and Y. Li, "A Novel Orientation Determination Approach of Mobile Robot Using Inertial and Magnetic Sensors," *IEEE Transactions on Industrial Electronics*, vol. 70, no. 4, pp. 4267–4277, 2023, doi: 10.1109/TIE.2022.3177762.

[16] B. Tu, B. Lu, and M. Piao, "Control of the Wheeled Bipedal Robot on Roads with Large and Unknown Inclination," in *Intelligent Robotics and Applications*, H. Yang, H. Liu, J. Zou, Z. Yin, L. Liu, G. Yang, X. Ouyang, and Z. Wang, Eds., Singapore: Springer Nature Singapore, 2023, pp. 282–293.

[17] S. Khan, J. Guivant, and X. Li, "Design and experimental validation of a robust model predictive control for the optimal trajectory tracking of a small-scale autonomous bulldozer," *Rob Auto Syst*, vol. 147, p. 103903, 2022, doi: https://doi.org/10.1016/j.robot.2021.103903.